Acta Polytechnica CTU Proceedings **53**:76–81, 2025
https://doi.org/10.14311/APP.2025.53.0076

Published by the Czech Technical University in Prague

MICRO-SCALE PROPERTIES OF CEMENT PASTES EXPOSED TO GAMMA RADIATION

Jiří Němeček[1a,*], Andrea Špaková[a], Jiří Němeček[2a], Patricie Halodová[b]

[a] *Czech Technical University in Prague, Faculty of Civil Engineering, Department of Mechanics, Thákurova 7, 166 29 Prague 6, Czech Republic*

[b] *Research Centre Řež, Hlavní 130 Řež, 250 68 Husinec, Czech Republic*

[*] corresponding author: jiri.nemecek@fsv.cvut.cz

Abstract. The extension of the lifetime of nuclear power plants is a critical issue today, raising concerns about the microscale mechanisms and mechanical changes in the individual phases of concrete that contribute to its macroscopic deterioration. Accurate quantification of these changes is essential for more reliable lifetime predictions. This paper investigates the effects of gamma irradiation on cement pastes exposed to varying relative humidity levels (RH = 11–100 %) using scanning electron microscopy (SEM) and nanoindentation. While SEM analysis did not reveal significant phase changes through image analysis, nanoindentation highlighted substantial differences in the mechanical properties of samples exposed to either low or high humidity or submerged in water during irradiation.

Keywords: Gamma irradiation, cement paste, humidity, nanoindentation, electron microscopy.

1. Introduction

Concrete, one of the most widely used man-made materials globally, is essential in nuclear power plants (NPPs) for biological shielding, reactor vessel foundations, spent fuel storage pools and radioactive waste storage containers. However, long-term degradation due to radiation and thermal strains has been extensively documented, resulting in a decline in macroscopic mechanical properties like compressive and tensile strengths, as well as the macroscopic modulus of elasticity, as summarized by [1] and [2]. This degradation ultimately leads to the deterioration of reinforced concrete structures in NPPs [3] otherwise designed for 80 years of operation [4].

The primary causes of this deterioration are neutron and gamma irradiation, along with heating and drying. During its lifetime, concrete used as a biological shield is exposed to 100–200 MGy of gamma irradiation and neutron fluxes of approximately 6×10^{19} n cm^{-2} (with $E > 0.1$ MeV) [1]. Neutron irradiation mainly impacts the aggregates, altering their crystallographic structure by amorfization of minerals and causing their radiation-induced volumetric expansion (RIVE) [5], while gamma irradiation affects the cement matrix by causing radiolysis of water and drying of Calcium-Silicate-Hydrates (C-S-H) [4]. Water radiolysis is a chemical reaction in which the interstitial liquid within the C-S-H gel breaks down, leading to the formation and accumulation of gases like hydrogen (H_2), other stable molecules (H_2O_2, H^+, OH^-), and highly unstable radicals ($H^\cdot$, $OH^\cdot$, e^-_{aq}). Hydrogen peroxide (H_2O_2) then reacts with calcium hydroxide (CH) and AFt phases, forming unstable products. Further reactions of these products result in the creation of calcium carbonate ($CaCO_3$) [6, 7].

However, there have been relatively few studies on gamma-irradiated concrete. Microscopic observations reveal that gamma irradiation decomposes evaporable water in cement pastes, and after prolonged exposure at high doses, up to 1 % of chemically bound water can also decompose [4]. During carbonation, vaterite and aragonite formed instead of calcite. Vaterite filled the pores around the C-S-H gel, increasing the stiffness and bending strength in cement pastes [7]. Nanoindentation at below 11 % relative humidity (RH) resulted in a 25 % increase in nanoindentation Young's modulus due to C-S-H gel densification, accompanied by microcracking that led to 17% reduction in microindentation Young's modulus [8]. Samples irradiated at 30–60 % RH showed minimal nanomechanical changes [8, 9], while those exposed to water experienced a 26 % decrease in Young's modulus and 9–10 % loss of Portlandite [8]. Scanning electron microscopy (SEM) and X-ray diffraction (XRD) analyses of samples exposed to doses up to 1 188 MGy showed decreasing crystalline phases, clinker decomposition, and microstructural damage starting at 130 MGy [10].

Hunnicutt et al. [11], who performed nanoindentation on synthetic C-S-H pellets exposed to gamma doses up to 0.784 MGy at 11 % RH, found minimal changes in micro-mechanical properties. More recently, [12] reported significant increases in nanoindentation Young's modulus (by 15–25 %) at higher exposure doses of 24 MGy and 189 MGy. Khumurovska et al. [9] studied mortar samples exposed to 12–15 MGy under 40–60 % RH for one year, observing negligible changes in Young's modulus and creep compliance. Similarly, Hilloulin et al. [13] performed

[1] Professor at Czech Technical University in Prague, ORCID: 0000-0002-3565-8182.

[2] Postdoctoral researcher at Czech Technical University in Prague, ORCID: 0000-0002-5635-695X.

	CaO	SiO_2	Al_2O_3	Fe_2O_3	MgO	Na_2O	K_2O	SO_3	Cl^-	MnO
(wt. %)	64.78	20.28	4.87	3.55	1.34	0.14	0.76	3.04	0.028	–

TABLE 1. Cement composition of CEM I 42.5R (XRF data provided by the manufacturer).

RH	11 %	33 %	76 %	96 %	100 %
Saturated salt solution	LiCl	$MgCl_2$	NaCl	KNO_3	-
Environment	Air	Air	Air	Air	Water

TABLE 2. Environmental conditions used in sample containers.

micro-indentation on samples subjected to gamma doses up to 0.257 MGy, with no changes in Young's modulus but a reported increase in creep modulus, although environmental conditions were not provided. The formation of bubbles and cracks due to the separation of chemically bound water was also observed by SEM at a dose of 290 MGy [10].

Since it is clear that macroscopic deterioration mechanisms of concrete begin at the micro-scale, conducting experiments at smaller scales is essential. In this context, nanoindentation is a valuable technique for characterizing the micro-mechanical properties of materials [14]. Given the limited research and the unclear role of RH, this study aims to clarify the influence of RH during gamma irradiation on the microstruture and micro-mechanical properties of cement paste using SEM and nanoindentation.

2. Experiments and methods

2.1. Samples and sample preparation

A cement paste with a water-cement ratio of 0.4 was prepared using Portland cement CEM I 42.5 R (Českomoravský cement, Czech Republic). The component composition of the Portland cement is detailed in Table 1. The mixture was poured into cylindrical plastic molds (27 mm diameter, 70 mm height) and vibrated. After 24 hours, the samples were demolded and stored in a 1 % lime water solution for 610 days (approximately 1.67 years). Once removed from the lime water, the samples were cut into slices of about 19 mm height using a diamond blade (Struers Secotom 50). The sliced samples were then used for two types of analyses: SEM analysis and nanoindentation under two types of exposition: irradiation and different RH. Several different RH levels: 11 %, 33 %, 76 %, 96 %, and 100 % (water) maintained by salt solutions were tested (see Table 2). The salt solutions were kept separate from the samples to prevent direct contact.

2.2. Gamma irradiation

Sample slices were placed in closed plastic containers under specific RH conditions provided by salt solutions (or water) and gamma irraditated. The gamma irradiation experiment was conducted at the Research Center Řež in the Czech Republic using a ^{60}Co radiation source. The samples in containers were left to stabilize at their respective RH conditions for 14 days. Half of the samples were then irradiated for 341 days, receiving a total dosage of 13.82 MGy and an average dose rate of 0.675–1.890 kGy h^{-1}. The second half of the control (non-irradiated) samples were kept under the same RH conditions but were not exposed to gamma radiation.

2.3. Scanning electron microscopy

The surfaces of the samples were polished using SiC foils with different grit sizes (#2000 to #4000) at varying speeds and pressure forces without any lubricant while constantly sweeping free particles out of the surface. After each polishing step, the samples were placed in isopropanol and an ultrasonic cleaner for 1 minute to remove any free particles.

A Phenom XL desktop SEM was utilized to analyze the phase composition of the cement paste samples. SEM imaging offers high-resolution capabilities, allowing for the clear identification of different phases within the cement paste. In typical cement paste, five key phases can be distinguished: inner and outer hydration products, Portlandite, residual clinker, and pores or cracks [15, 16]. Back-scattered electron (BSE) images were captured at 900× magnification, covering an area of $298 \times 298\,\mu m^2$ with a pixel resolution of 146 nm. The SEM was operated at an accelerating voltage of 15 kV. For each sample, ten images were taken, covering a total area of 0.888 mm^2. These images were then saved into 8-bit grayscale format, with pixel intensity values ranging from 0 to 255, and further analyzed for phase composition using ImageJ software.

2.4. Nanoindentation

After irradiation and exposition to different RH, samples were stored in boxes with silica gel (≈ 11 % RH) to prevent further hydration and carbonation until tested.

Nanoindentation at ambient conditions (temperature ≈ 23 °C, RH ≈ 40–50 %) was carried out using Hysitron TI-980 Triboindenter equipped with a Berkovich diamond tip and using the accelerated property mapping mode (XPM). A grid of 22×22 indents, spaced 2.5 µm apart, was applied to each sample.

The indentation protocol followed a trapezoidal load function. The load segment involved linear loading for

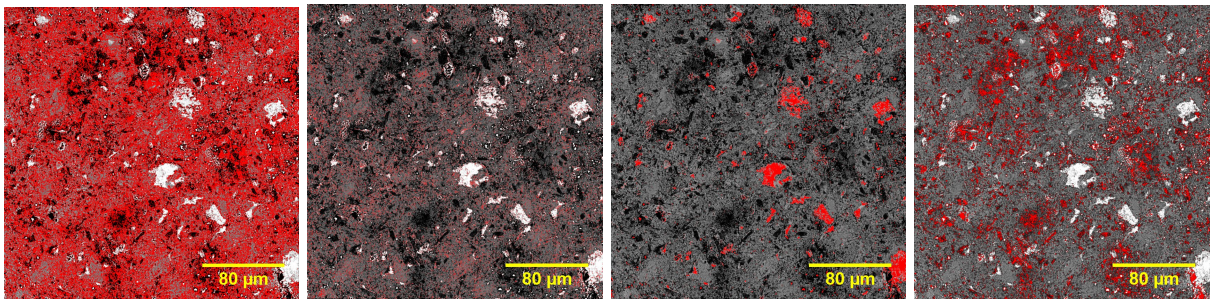

a) b) c) d)

Figure 1. Example of phase separation for the irradiated sample (RH=76 %) using image analysis for individual phases: a) inner-outer product, b) Portlandite, c) clinker, d) pores and cracks.

RH	11 %	33 %	76 %	96 %	100 %
Clinker IR	4.09 ± 0.86	5.11 ± 1.20	4.85 ± 0.88	4.63 ± 1.11	3.50 ± 0.94
Clinker NR	4.52 ± 0.75	4.61 ± 0.99	4.34 ± 1.34	4.31 ± 0.80	3.60 ± 0.89
Portlandite IR	5.60 ± 0.43	7.53 ± 0.46	4.52 ± 0.36	4.83 ± 0.20	6.64 ± 1.24
Portlandite NR	5.02 ± 0.68	8.18 ± 0.65	5.17 ± 0.21	5.75 ± 0.30	7.80 ± 0.34
Inner-outer product IR	81.01 ± 0.94	78.90 ± 0.99	81.13 ± 1.00	83.61 ± 1.22	82.61 ± 2.09
Inner-outer product NR	81.28 ± 0.78	77.61 ± 1.26	80.93 ± 1.54	81.61 ± 1.13	81.39 ± 0.95
Pores and cracks IR	9.30 ± 0.78	8.46 ± 1.20	9.50 ± 0.69	7.42 ± 0.62	7.25 ± 0.80
Pores and cracks NR	9.18 ± 0.69	9.60 ± 0.88	9.56 ± 0.58	8.22 ± 0.83	7.20 ± 0.61

Table 3. Image analysis results: the table shows volumetric ratios (vol. %) of the given phases for the irradiated sample (IR) and the non-irradiated sample (NR).

0.1 seconds up to a maximum load of 1.5 mN, holding the load for 0.1 seconds, and then unloading linearly for 0.1 seconds.

The elastic properties were evaluated using the unloading segment of the load-displacement curve, based on the method of Oliver and Pharr [14]. The reduced modulus, E_r, and hardness, H, were determined using the equations:

$$E_r = \frac{S\sqrt{\pi}}{2\beta\sqrt{A_c}}, \tag{1}$$

$$H = \frac{P_{max}}{A_c}, \tag{2}$$

where A_c represents the projected contact area of the tip, S is the elastic unloading stiffness, β is the correction factor for the tip geometry (with $\beta = 1.034$ for Berkovich), and P_{max} is the maximum load. The reduced modulus E_r reflects the combined elastic response of both the nanoindentation tip and the material. The Young's modulus, E, of the (isotropic) material can then be determined from the following relationship:

$$\frac{1}{E_r} = \frac{1-\nu^2}{E} + \frac{1-\nu_i^2}{E_i}, \tag{3}$$

where E_i and ν_i are Young's modulus and Poisson's ratio of the nanoindentation tip, respectively. For a diamond tip, these values are typically $E_i = 1\,141$ GPa and $\nu_i = 0.07$. The Poisson's ratio of the sample, ν, was assumed to be 0.2 ([16, 17]).

3. Results and Discussion

3.1. SEM and image analysis

For the analysis of sample phase composition, SEM images were segmented into five primary phases: residual clinker, Portlandite, inner product, outer product, and cracks/pores, using pixel color thresholding. However, due to overlapping grayscale values between the inner and outer product phases [16], these two were grouped and analyzed as a combined "inner-outer product" phase. An example of this segmentation process is shown for the irradiated sample (RH=100 %) in Figure 1. The grayscale threshold boundaries used for segmentation were: residual clinker (255–185), Portlandite (184–150), inner-outer product (149–41), and pores/cracks (40–0). The average values and standard deviations for each irradiated and non-irradiated sample are provided in Table 3.

The image analysis results reveal minimal differences between irradiated and non-irradiated samples across all RH levels, with almost negligible changes observed in the inner-outer product phase. At 100 % RH, there is a slight decrease of approximately 1 % in residual clinker and about 2 % in the pores/cracks phase compared to other RH conditions, suggesting these changes are due to ongoing hydration rather than irradiation. A minor reduction in Portlandite content (1.5–3.5 %) was noted at 33 %, 76 %, 96 %, and water, indicating potential decomposition from irradiation, consistent with previous studies [8, 10]. However, these changes are within the method's accuracy, and thermogravimetric analysis is planned to be con-

ducted for more precise Portlandite estimation in the future. Additionally, SEM-BSE images were analyzed for radiation-induced crack formation, but no cracks were detected in either irradiated or non-irradiated samples. This contrasts with findings from other studies. For example, crack formation was observed by Łowińska-Kluge and Piszora [10] after exposure to a gamma dose of 130 MGy, significantly higher than the dose used in our study. Similarly, Němeček et al. [8] reported crack formation in irradiated samples, though this was primarily due to prolonged exposure to the SEM vacuum chamber and not the gamma radiation exposure.

3.2. Nanoindentation

A continuous spectrum of E values from 10 GPa to 130 GPa was obtained showing the large differences between individual mechanically dissimilar phases [17, 18]. Based on the correspondence with the phase locations observed by SEM, typical values of E were found as: residual clinker E = 50–130 GPa, Portlandite E = 36–43 GPa, inner product E = 26–38 GPa, outer product E = 19–26 GPa, low stiffness phase E < 15 GPa), values similar to other studies [16–18]. The typical load-displacement diagrams of these phases separated by post-indentation SEM imaging are shown in Figure 2. In order to reveal individual phase properties, all indents from a sample were merged together, and frequency density plots were created for each sample. An example of these plots is shown in Figure 3. Since the spectrum of E is continuous with a single major peak, no distinction was made between individual hydration phases and the hydrates were collectively called 'main hydrates', meaning responses from inner-outer products and Portandite were grouped into a single mechanical phase. The second phase was created by non-hydrated residual clinker. The two mechanical phases were separated with a statistical deconvolution method, which assumed overlapping Gaussian distributions of individual phases. More details of the method can be found in [17–19]. Based on these results, the difference in micro-mechanical behavior between irradiated and non-irradiated samples was analyzed and summarized in Figure 4.

The effect of irradiation is evident in Figure 4. Samples stored at low RH (11 %) showed a 9.5 % increase in E compared to non-irradiated samples and a 19.9 % increase compared to irradiated samples stored at medium RH levels. This increase is likely due to drying shrinkage, leading to the densification and compaction of C–S–H [20, 21]. In irradiated samples, water radiolysis likely depletes water from the interlayer space, further promoting densification. This trend aligns with other studies on well-matured cement pastes exposed to low RHs [8, 12]. Studies on younger samples (irradiated at 4 weeks of age) demonstrated an even higher increase in E (+24.8 %) with a smaller radiation dose of 2.88 MGy [8]. These findings suggest that the hydration degree at the onset of irradiation significantly influences the radiolysis process and the subsequent C–S–H compaction. It is

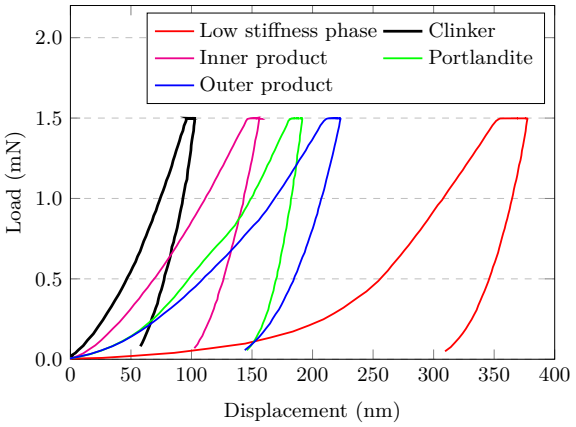

Figure 2. An example of typical load-displacement curves of main phases measured for irradiated sample (RH=76 %).

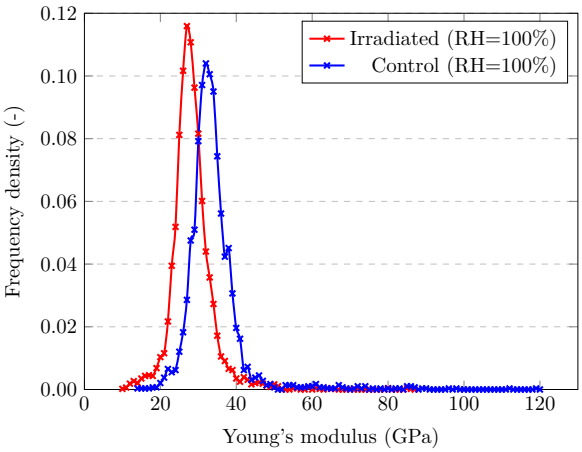

Figure 3. A typical example of frequency plots of Young's modulus for irradiated and non-irradiated (control) sample (RH=100 %).

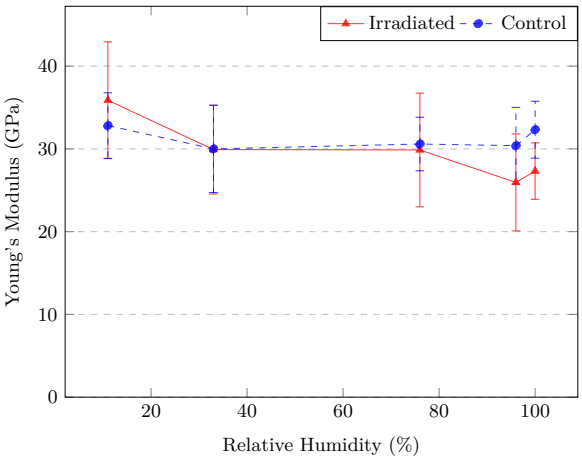

Figure 4. Summary of Young's moduli of main hydrates for irradiated and non-irradiated (control) samples stored at different RH levels.

important to note that the localized increase in E is accompanied by drying microcracking in the samples, which ultimately leads to a reduction in mechanical properties at larger scales [8].

Samples stored at medium RHs (33 %, 76 %) exhibited minimal differences between irradiated and non-irradiated states, indicating that water loss due to radiolysis is likely offset by the available moisture in the container. These results are consistent with previous studies on gamma doses ranging from 0.257 MGy to 15 MGy [8, 9, 13].

The samples stored at high RH levels (96 % and water-saturated) showed the most significant deterioration in mechanical properties due to irradiation. The decrease in E was found to be significant (14.6 % at 96 % RH and 15.5 % in water). This deterioration is likely caused by water radiolysis, although the precise mechanism remains unclear. Similar findings were reported by Němeček et al. [8] for 28-day-old samples irradiated with a dose of 2.88 MGy. Future studies by X-ray diffraction, thermogravimetry, and porosity measurements are planned to disclose the mechanism.

The residual clinker properties, as for a crystalline phase, were not impacted by gamma radiation. It aligns with the findings reported by Rosseel et al. [1]. In their study, it was noted that gamma radiation typically does not significantly affect the crystalline phases of concrete, such as residual clinker, which remains stable under gamma irradiation.

4. Conclusions

The lifetime extension of nuclear power plants relies on the description of deterioration mechanisms in concrete used for biological shield and containment structures and a precise quantification of mechanical properties of the micro-scale phases. Environmental exposure significantly influences the evolution of properties. This study investigated gamma-irradiated ordinary cement paste with total absorbed dose of 13.82 MGy exposed to five different RH levels (11–100 %) using scanning electron microscopy and nanoindentation. Based on the observations and measurements the following conclusions were drawn.

- Insignificant changes in volume fractions of C-S-H hydrated phases were observed by SEM image analysis across all RH levels.
- A 1.5–3.5 % decrease in Portlandite phase was observed in medium to high (33–100 %) humidities, indicating its degradation due to gamma irradiation.
- No substantial crack formation in either the irradiated or non-irradiated samples was observed by SEM and image analysis.
- Nanoindentation of samples irradiated at low RH (11 %) revealed a 9.3 % increase in Young's modulus for the main hydrates. This increase is likely due to a combination of water radiolysis and drying, which may have resulted in the removal of water from the interlayer space and compaction of the C-S-H gel.
- Samples irradiated at medium RHs (33 %, 76 %) did not exhibit a significant change in nanomechanical response.
- Samples irradiated at high RHs exhibited a ≈15 % decrease in Young's modulus, highlighting the significant impact of gamma radiation and water radiolysis on the material's mechanical properties.

Acknowledgements

This work was financially supported by the project of the Czech Science Foundation grant number 23-05435S. The presented results were obtained using the CICRR infrastructure, which is financially supported by the Ministry of Education and Culture – project LM2023041.

References

[1] T. Rosseel, I. Maruyama, Y. Le Pape, et al. Review of the current state of knowledge on the effects of radiation on concrete. *Journal of Advanced Concrete Technology* **14**(7):368–383, 2016. https://doi.org/10.3151/jact.14.368

[2] K. Field, I. Remec, Y. L. Pape. Radiation effects in concrete for nuclear power plants – Part I: Quantification of radiation exposure and radiation effects. *Nuclear Engineering and Design* **282**:126–143, 2015. https://doi.org/10.1016/j.nucengdes.2014.10.003

[3] K. Park, H.-T. Kim, T.-H. Kwon, E. Choi. Effect of neutron irradiation on response of reinforced concrete members for nuclear power plants. *Nuclear Engineering and Design* **310**:15–26, 2016. https://doi.org/10.1016/j.nucengdes.2016.09.034

[4] O. Kontani, S. Sawada, I. Maruyama, et al. Evaluation of irradiation effects on concrete structure: Gamma-ray irradiation tests on cement paste. In *ASME Power Conference*, vol. 56062, p. V002T07A002. American Society of Mechanical Engineers, 2013. https://doi.org/10.1115/POWER2013-98099

[5] I. Maruyama, O. Kontani, M. Takizawa, et al. Development of soundness assessment procedure for concrete members affected by neutron and gamma-ray irradiation. *Journal of Advanced Concrete Technology* **15**(9):440–523, 2017. https://doi.org/10.3151/jact.15.440

[6] P. Bouniol, A. Aspart. Disappearance of oxygen in concrete under irradiation: the role of peroxides in radiolysis. *Cement and Concrete Research* **28**(11):1669–1681, 1998. https://doi.org/10.1016/S0008-8846(98)00138-0

[7] I. Maruyama, S. Ishikawa, J. Yasukouchi, et al. Impact of gamma-ray irradiation on hardened white Portland cement pastes exposed to atmosphere. *Cement and Concrete Research* **108**:59–71, 2018. https://doi.org/10.1016/j.cemconres.2018.03.005

[8] J. Němeček, P. Trávníček, M. Keppert, et al. Nanomechanical analysis of Gamma-irradiated cement paste exposed to different humidities. *Construction and Building Materials* **393**:131969, 2023. https://doi.org/10.1016/j.conbuildmat.2023.131969

[9] Y. Khmurovska, P. Štemberk, S. Sikorin, et al. Effects of gamma-ray irradiation on hardened cement mortar. *International Journal of Concrete Structures and Materials* **15**(1):1–14, 2021. https://doi.org/10.1186/s40069-020-00452-7

[10] A. Lowinska-Kluge, P. Piszora. Effect of gamma irradiation on cement composites observed with XRD and SEM methods in the range of radiation dose 0-1409 MGy. *Acta Physica Polonica A* **114**(2):399–411, 2008. https://doi.org/10.12693/APhysPolA.114.399

[11] W. Hunnicutt, E. Rodriguez, P. Mondal, Y. Le Pape. Examination of gamma-irradiated calcium silicate hydrates. Part II: Mechanical properties. *Journal of Advanced Concrete Technology* **18**(10):558–570, 2020. https://doi.org/10.3151/jact.18.558

[12] A. Baral, E. T. Rodriguez, W. A. Hunnicutt, et al. Ultra-high gamma irradiation of calcium silicate hydrates: Impact on mechanical properties, nanostructure, and atomic environments. *Cement and Concrete Research* **158**:106855, 2022. https://doi.org/10.1016/j.cemconres.2022.106855

[13] B. Hilloulin, M. Robira, A. Loukili. Coupling statistical indentation and microscopy to evaluate micromechanical properties of materials: Application to viscoelastic behavior of irradiated mortars. *Cement and Concrete Composites* **94**:153–165, 2018. https://doi.org/10.1016/j.cemconcomp.2018.09.008

[14] W. C. Oliver, G. M. Pharr. An improved technique for determining hardness and elastic modulus using load and displacement sensing indentation experiments. *Journal of materials research* **7**(6):1564–1583, 1992. https://doi.org/10.1557/JMR.1992.1564

[15] K. L. Scrivener. Backscattered electron imaging of cementitious microstructures: understanding and quantification. *Cement and Concrete Composites* **26**(8):935–945, 2004. Scanning electron microscopy of cements and concretes. https://doi.org/10.1016/j.cemconcomp.2004.02.029

[16] J. Němeček, J. Lukeš, J. Němeček. High-speed mechanical mapping of blended cement pastes and its comparison with standard modes of nanoindentation. *Materials Today Communications* **23**:100806, 2020. https://doi.org/10.1016/j.mtcomm.2019.100806

[17] G. Constantinides, F.-J. Ulm. The nanogranular nature of C–S–H. *Journal of the Mechanics and Physics of Solids* **55**(1):64 – 90, 2007. https://doi.org/10.1016/j.jmps.2006.06.003

[18] G. Constantinides, F.-J. Ulm. The effect of two types of C-S-H on the elasticity of cement-based materials: Results from nanoindentation and micromechanical modeling. *Cement and Concrete Research* **34**(1):67–80, 2004. https://doi.org/10.1016/S0008-8846(03)00230-8

[19] J. Němeček, V. Králík, J. Vondřejc. Micromechanical analysis of heterogeneous structural materials. *Cement and Concrete Composites* **36**:85–92, 2013. https://doi.org/10.1016/j.cemconcomp.2012.06.015

[20] J. Němeček, J. Maňák, J. Němeček, T. Krejčí. Effect of vacuum and Focused Ion Beam generated heat on fracture properties of hydrated cement paste. *Cement and Concrete Composites* **100**:139–149, 2019. https://doi.org/10.1016/j.cemconcomp.2019.03.027

[21] P. Suwanmaneechot, A. Aili, I. Maruyama. Creep behavior of C-S-H under different drying relative humidities: Interpretation of microindentation tests and sorption measurements by multi-scale analysis. *Cement and Concrete Research* **132**:106036, 2020. https://doi.org/10.1016/j.cemconres.2020.106036